**The 14th International Topical Meeting on Nuclear Reactor Thermalhydraulics, NURETH-14**
**Toronto, Ontario, Canada, September 25-30, 2011**

**NURETH14-308**

# INVESTIGATION ON THE INFLUENCE OF PRESSURE AND TEMPERATURE ON THE IGNITION LIMITS OF HYDROGEN INSIDE RECOMBINERS

**N. Meynet[1], S. Engelhardt[1], A. Bentaib[1]**
[1] Institut de Radioprotection et de Sûreté Nucléaire (IRSN)
DSR/SAGR/BPhAG - BP 17, 92262 Fontenay aux Roses, France
*Corresponding author: nicolas.meynet@irsn.fr

## Abstract

Passive Auto-catalytic Recombiners (PARs) are used to avoid excessive hydrogen accumulation inside the reactor containment in case of severe accident. Their behavior is based on the exothermic recombination of hydrogen into steam in presence of oxygen. This surface mechanism leads to an overheating of the catalytic plates and activates natural convection-driven circulation of gases in contact with the catalyst. The heat source induced by the PAR activity can then create local conditions for hydrogen gaseous combustion, as igniters do.

This paper deals with the numerical simulation of the impact of thermal-hydraulic conditions on PAR hydrogen ignition limits. The separated effects of three main parameters (steam, pressure and temperature) are analyzed. Calculations using an IRSN dedicated CFD code, reveal that hydrogen ignition inside recombiners can be significantly accelerated or delayed according to the reactor containment atmosphere.

## Introduction

In case of a severe accident with core meltdown in a nuclear reactor, the interaction of the hot core with the cooling water can generate large amounts of hydrogen. Hydrogen can also result from the oxidation of metals present in the corium pool or in the basemat during the molten corium-concrete interaction phase. This hydrogen is transferred into the containment (and transported therein) by convection loops arising essentially from condensation of steam released via the break in the reactor cooling system or during corium-concrete interaction. Depending on mixing in the containment atmosphere, the distribution of hydrogen is more or less homogeneous. If considerable hydrogen stratification exists, then local concentration of hydrogen may become substantial, and may exceed the lower flammability limit. In case of ignition, the subsequent pressure loads may adversely affect the containment.

To limit the hydrogen concentration in the containment, several methods can be proposed. For pressurized water reactors (PWRs), the hydrogen mitigation strategy usually consists in combining a large free volume to allow atmosphere dilution, a high value of the containment design pressure and the use of means like passive autocatalytic recombiners to consume hydrogen. This strategy has been adopted in all French PWRs.

To support this decision, specific experimental set-ups have been conducted to investigate the PARs efficiency under representative severe accident conditions. Thus, it appeared that for specific conditions, PARs could induce combustion, as igniters do. Among these experiments, the H2PAR program [1], conducted by IRSN (formerly IPSN) and co-funded by EDF, addressed the characterization of PAR ignition conditions, as illustrated in Figure 1.

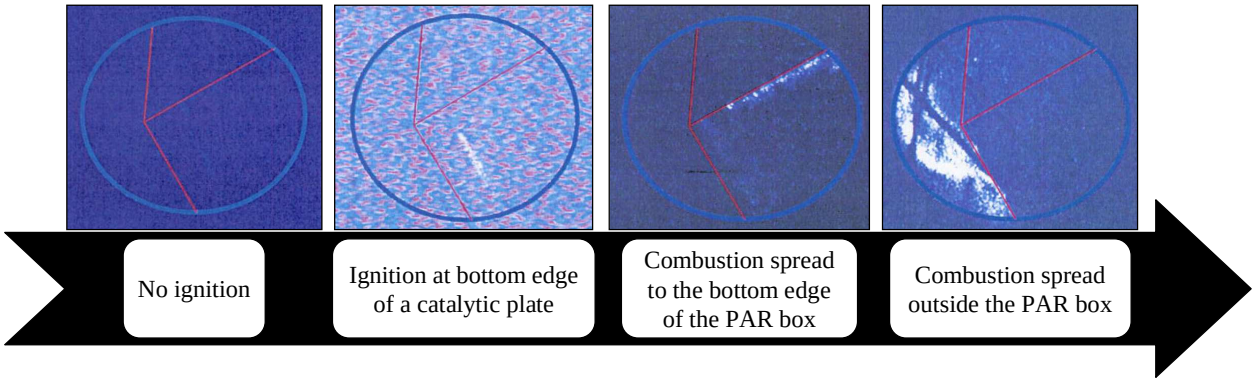


Figure 1 Visualization by UV camera of the hydrogen flame propagation during a H2PAR experimental test (red lines: contour of the PAR box, blue circle: camera scope)

The numerous tests carried out at atmospheric pressure with different $H_2$/Air/$H_2O$ mixtures showed that hydrogen ignition induced by recombiners can occur, but under specific concentrations limits. The KALI-H2 program [2] conducted by CEA, and more recently the OECD THAI project [3], have corroborated these results, so that experimental PARs hydrogen ignition limit can be defined at:

- around 6.0 vol.% of hydrogen in dry air,
- around 7.5 vol.% of hydrogen with 25 vol.% of steam,
- around 9.0 vol.% of hydrogen with 45 vol.% of steam.

Based on this experimental data, it seems that hydrogen ignition induced by recombiners occurs for low hydrogen concentrations, leading to relatively low overpressure. Hence, PARs hydrogen ignition could have a beneficial effect [4]. Nonetheless, these experiments' results need to be corroborated by more detailed experiments and by refined modeling of phenomena occurring in PARs.

This paper presents the numerical simulation of the separated effects of steam, pressure and temperature on the hydrogen ignition limit inside PARs. The calculations are performed with a dedicated CFD code, named SPARK. This numerical tool which is developed at IRSN is based on a detailed PAR modeling including multicomponent transport, and complex chemistry in the gas phase and on the catalytic surface. In this study, we analyze numerically the impact of thermal-hydraulic conditions on the PAR hydrogen ignition limits, with an accelerated or a delayed ignition according to steam concentration, pressure, or temperature.

## 1. SPARK code

In this section, we describe the numerical tool developed by IRSN dedicated to catalytic reactor-type applications. Its name SPARK is the acronym of Simulation for Passive Autocatalytic Recombiners' risK. This code solves the two-dimensional steady-state Navier-Stokes equations in the vorticity-

velocity formulation by including complex gas phase and surface chemistry, multi-component transport, and heat radiation [5][6].

## 1.1 Numerical domain

The numerical domain is derived from the box-type PARs with row of vertical catalytic sheets as illustrated in Figure 2. We suppose infinitely thin catalytic plates, so that solid heat conduction is neglected. Moreover, external heat losses are not taken into account. As a result, the flow is supposed to be symmetrical and the numerical domain is reduced to a half-channel between two catalytic plates in the median plane (Figure 2).

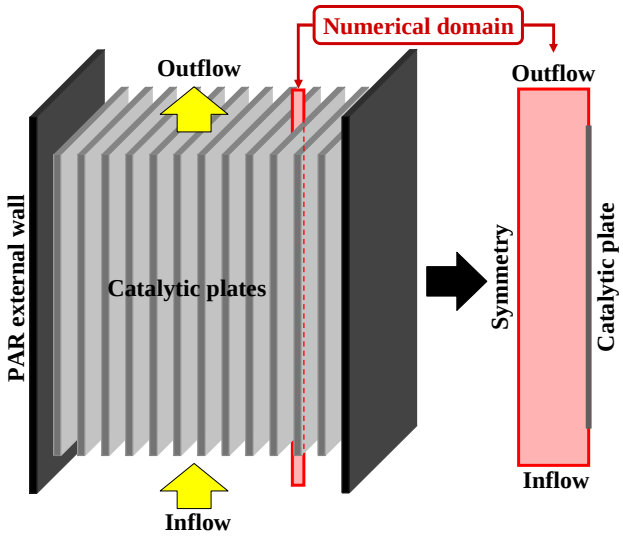


Figure 2 Schematic of catalytic sheets inside PARs (left) and numerical domain (right)

## 1.2 Governing equations

The governing equations are based on the modified vorticity-velocity formulation of the Navier-Stokes equations [7] for two-dimensional planar reactive flows. The gas phase equations are written as follows:

- Horizontal velocity

$$\partial^2_{xx}u+\partial^2_{yy}u=\partial_y\omega-\partial(\frac{u}{\rho}\partial_x\rho+\frac{v}{\rho}\partial_y\rho), \tag{1}$$

- Vertical velocity

$$\partial^2_{yy}v=-\partial^2_{xy}u-\partial_y(\frac{u}{\rho}\partial_x\rho+\frac{v}{\rho}\partial_y\rho), \tag{2}$$

- Vorticity

$$\begin{aligned}&\partial^2_{xx}(\mu\omega)+\partial^2_{yy}(\mu\omega)=\rho u\,\partial_x\omega+\rho v\,\partial_y\omega+2\partial_x\mu\,\partial_y(\partial_x u+\partial_y v)-2\partial_y\mu\,\partial_x(\partial_x u+\partial_y v)\\&+\partial_y\rho\,\partial_x(u^2/2)-\partial_x\rho\,\partial_y(v^2/2)+2\partial_y u\,\partial^2_{xx}\mu-2\partial_x v\,\partial^2_{yy}\mu-2\partial_x u\,\partial^2_{yx}\mu+2\partial_y v\,\partial^2_{xy}\mu+\partial_x\rho\,g,\end{aligned} \tag{3}$$

- Gaseous species mass

$$\rho u\,\partial_x Y_k + \rho v\,\partial_y Y_k = -\partial_x(\rho Y_k U_k) - \partial_y(\rho Y_k V_k) + M_k \omega_k \quad \text{for} \quad k = 1\ldots n, \tag{4}$$

- Energy

$$\rho c_p u\,\partial_x T + \rho c_p v\,\partial_y T = \partial_x(\lambda \partial_x T) + \partial_y(\lambda \partial_y T) - \sum_{k=1}^{n} \rho c_{pk} Y_k (U_k \partial_x T + V_k \partial_y T) - \sum_{k=1}^{n} h_k M_k \omega_k, \tag{5}$$

where $\rho$ is the density, u and v the horizontal and vertical velocities, T the temperature, $Y_k$ the mass fraction of the $k^{th}$ species, $\partial_x$ the space derivative operator, g the gravitational acceleration, $\mu$ the shear viscosity of the mixture, $U_k$ and $V_k$ the horizontal and vertical diffusion velocities of the $k^{th}$ species, $M_k$ the molar mass of the $k^{th}$ species, $\omega_k$ the gas phase molar production rate of the $k^{th}$ species, $c_p$ the specific constant pressure heat capacity of the mixture, $\lambda$ the thermal conductivity of the mixture, n the number of gaseous species, $h_k$ the specific enthalpy of the $k^{th}$ species and $c_{pk}$ its specific constant pressure heat capacity. The vorticity $\omega$ is classically defined by:

$$\omega = \partial_y u - \partial_x v. \tag{6}$$

One additional equation expresses the absence of surface species inside the gas flow:

$$\sigma_k = 0 \quad \text{for} \quad k = 1\ldots \hat{n}, \tag{7}$$

where $\sigma_k$ is the site fraction occupancy of the $k^{th}$ species, and $\hat{n}$ the number of surface species. Finally, the ideal gas law completes the governing equations:

$$\rho = \frac{p_0 \overline{M}}{RT}, \tag{8}$$

where $\overline{M}$ is the molar mass of the mixture, R the universal gas constant, and $p_0$ the ambient pressure.

## 1.3 Boundary conditions

### 1.3.1 Catalytic surface

The boundary condition on the catalytic surface expresses the conservation of species mass and energy through the solid-gas reactive interface, and the no-slip conditions. These balance equations may be written as follows:

- Horizontal and vertical velocities

$$u = v = 0, \tag{9}$$

- Gaseous species mass

$$\rho Y_k U_k = -M_k \hat{\omega}_k \quad \text{for} \quad k = 1\ldots n, \tag{10}$$

- Surface species mass (no mass accumulation on the catalytic surface)

$$\hat{\omega}_k = 0 \quad \text{for} \quad k = n+1\ldots n+\hat{n}, \tag{11}$$

- Energy

$$\lambda \partial_x T = -\sum_{k=1}^{n} h_k M_k \hat{\omega}_k - q^{rad}, \tag{12}$$

where $\hat{\omega}_k$ is the surface molar production rate of the $k^{th}$ species and $q^{rad}$ the radiative heat flux.

### 1.3.2 Inlet

The boundary conditions on the inlet are the estimated experimental conditions at PAR inlet. We consider uniform profiles for all the variables:

$$u = 0, \quad v = v_{in}, \quad \omega = \partial_y u - \partial_x v, \quad T = T_{in}, \quad \rho Y_k^{in} v_{in} = \rho Y_k \left(v + V_k\right) \quad \text{for} \quad k = 1 \ldots n, \tag{13}$$

where $v_{in}$ is the inlet vertical velocity, $Y_k^{in}$ the inlet mass fraction of the $k^{th}$ species, and $T_{in}$ the inlet temperature.

### 1.3.3 Outlet

The boundary condition on the outlet sets the vertical derivatives to zero:

$$u = 0, \quad \partial_y v = 0, \quad \partial_y \omega = 0, \quad \partial_y T = 0, \quad \partial_y Y_k = 0 \quad \text{for} \quad k = 1 \ldots n. \tag{14}$$

### 1.3.4 Symmetry

The boundary condition on the symmetry axis sets the horizontal derivatives to zero:

$$u = 0, \quad \partial_x v = 0, \quad \omega = 0, \quad \partial_x T = 0, \quad \partial_x Y_k = 0 \quad \text{for} \quad k = 1 \ldots n. \tag{15}$$

## 1.4 Transport

The different transport coefficients which appear in the governing equations (shear viscosity, conductivity, diffusion coefficients) are derived from the kinetic theory of gases [9], and are evaluated using multicomponent transport algorithms [10]. The species diffusion velocities are then given by:

$$U_k = -\sum_{l=1}^{n} D_{kl} \partial_x X_l - \theta_k \partial_x (\log T) \quad \text{for} \quad k = 1 \ldots n, \tag{16}$$

where $X_l$ is the molar fraction of the $l^{th}$ species, $D_{kl}$ the species diffusion coefficients, and $\theta_k$ the thermal diffusion coefficient of the $k^{th}$ species. This definition includes the multi-component diffusion (i.e. each species diffuses in relation to all the other species) and the thermal species diffusion (or Soret effect).

## 1.5 Chemical kinetics

The molar gas phase and surface production rates are derived from detailed chemical mechanisms. The molar production rate of each species in the gas or on the surface results from the sum of its

molar production rates over the reactions described in the next tables. The gas phase chemical kinetics [11] for hydrogen combustion in air includes 9 gaseous species for 19 reactions (Table 1). The surface chemical kinetics [12] for catalytic hydrogen recombination on platinum includes 5 surface species and 6 gaseous species for 13 reactions (Table 2). The alumina-supported Platinum catalyst is simulated by a polycrystalline platinum layer with a surface site density taken as $S_0 = 2.06\ 10^{-9}$ mol/cm$^2$ [13]. Both chemical mechanisms have been successfully validated for applications in a catalytic channel combustor [14]. Their combination allows a relevant estimation of the ignition distance inside a catalytic reactor for $H_2$/Air mixtures.

Table 1 Gas phase chemical mechanism

| $H_2/O_2$ reactions | | A | b | E |
|---|---|---|---|---|
| 1. | $H + O_2 \Leftrightarrow O + OH$ | $2.00\ 10^{14}$ | 0.00 | 16802.10 |
| 2. | $O + H_2 \Leftrightarrow H + OH$ | $5.06\ 10^{4}$ | 2.67 | 6285.85 |
| 3. | $H_2 + OH \Leftrightarrow H_2O + H$ | $1.00\ 10^{08}$ | 1.60 | 3292.28 |
| 4. | $OH + OH \Leftrightarrow O + H_2O$ | $1.50\ 10^{09}$ | 1.14 | 100.38 |
| 5[b]. | $H + H + M \Leftrightarrow H_2 + M$ | $1.80\ 10^{18}$ | -1.00 | 0.00 |
| 6[b]. | $O + O + M \Leftrightarrow O_2 + M$ | $2.90\ 10^{17}$ | -1.00 | 0.00 |
| 7[b]. | $H + OH + M \Leftrightarrow H_2O + M$ | $2.20\ 10^{22}$ | -2.00 | 0.00 |
| $HO_2$ reactions | | A | b | E |
| 8[b]. | $H + O_2 + M \Leftrightarrow HO_2 + M$ | $2.30\ 10^{18}$ | -0.80 | 0.00 |
| 9. | $HO_2 + H \Leftrightarrow H_2 + O_2$ | $2.50\ 10^{13}$ | 0.00 | 693.12 |
| 10. | $HO_2 + H \Leftrightarrow OH + OH$ | $1.50\ 10^{14}$ | 0.00 | 1003.82 |
| 11. | $HO_2 + H \Leftrightarrow H_2O + O$ | $3.00\ 10^{13}$ | 0.00 | 1720.84 |
| 12. | $HO_2 + O \Leftrightarrow OH + O_2$ | $1.80\ 10^{13}$ | 0.00 | -406.31 |
| 13. | $HO_2 + OH \Leftrightarrow H_2O + O_2$ | $6.00\ 10^{13}$ | 0.00 | 0.00 |
| $H_2O_2$ reactions | | A | b | E |
| 14. | $HO_2 + HO_2 \Leftrightarrow H_2O_2 + O_2$ | $2.50\ 10^{11}$ | 0.00 | -1242.83 |
| 15[b]. | $OH + OH + M \Leftrightarrow H_2O_2 + M$ | $3.25\ 10^{22}$ | -2.00 | 0.00 |
| 16. | $H_2O_2 + H \Leftrightarrow H_2O + OH$ | $1.00\ 10^{13}$ | 0.00 | 3585.09 |
| 17. | $H_2O_2 + H \Leftrightarrow H_2 + HO_2$ | $1.70\ 10^{12}$ | 0.00 | 3752.39 |
| 18. | $H_2O_2 + O \Leftrightarrow OH + HO_2$ | $2.80\ 10^{13}$ | 0.00 | 6405.35 |
| 19. | $H_2O_2 + OH \Leftrightarrow H_2O + HO_2$ | $5.40\ 10^{12}$ | 0.00 | 1003.82 |

[a] Reaction rate coefficients: $k = A\ T^b \exp(-E/RT)$ with A [mole-cm-Kelvin-sec] and E [cal/mole].
[b] Third body efficiencies: $\alpha_{H2O} = 6.5$, $\alpha_{O2} = 0.4$, and $\alpha_{N2} = 0.4$.

Table 2 Surface chemical mechanism

| Adsorption Reactions | | s | E |
|---|---|---|---|
| 1[b]. | $H_2 + 2\ Pt^{(s)} \rightarrow 2H^{(s)}$ | 0.046 | - |
| 2. | $H + Pt^{(s)} \rightarrow H^{(s)}$ | 1.0 | - |
| 3[c]. | $O_2 + 2\ Pt^{(s)} \rightarrow 2\ O^{(s)}$ | 0.07 | - |
| 4. | $O + Pt^{(s)} \rightarrow O^{(s)}$ | 1.0 | - |
| 5. | $H_2O + Pt^{(s)} \rightarrow H_2O^{(s)}$ | 0.75 | - |
| 6. | $OH + Pt^{(s)} \rightarrow OH^{(s)}$ | 1.0 | - |
| Surface Reactions | | A | E |
| 7. | $H^{(s)} + O^{(s)} \Leftrightarrow OH^{(s)} + Pt^{(s)}$ | $3.7\ 10^{21}$ | 2749 |
| 8. | $H^{(s)} + OH^{(s)} \Leftrightarrow H_2O^{(s)} + Pt^{(s)}$ | $3.7\ 10^{21}$ | 4183 |
| 9. | $OH^{(s)} + OH^{(s)} \Leftrightarrow H_2O^{(s)} + O^{(s)}$ | $3.7\ 10^{21}$ | 11520 |
| Desorption Reactions | | A | E |
| 10. | $H^{(s)} + H^{(s)} \rightarrow H_2 + 2\ Pt^{(s)}$ | $3.7\ 10^{21}$ | $16109 - 1439\ \sigma_H$ |
| 11. | $O^{(s)} + O^{(s)} \rightarrow O_2 + 2\ Pt^{(s)}$ | $3.7\ 10^{21}$ | $50956 - 14340\ \sigma_O$ |
| 12. | $H_2O^{(s)} \rightarrow H_2O + Pt^{(s)}$ | $1.0\ 10^{13}$ | 9632 |
| 13. | $OH^{(s)} \rightarrow OH + Pt^{(s)}$ | $1.0\ 10^{13}$ | 46080 |

[a] Reaction rate coefficients: $k = A \exp(-E/RT)$ with A [mole-cm- Kelvin-sec] and E [cal/mole].
[b] The hydrogen adsorption is first order with respect to platinum.
[c] The oxygen sticking coefficient is temperature dependent: $\gamma_{O2} = 0.07(T_0/T)$ with $T_0$=300 K.

## 1.6 Numerical method

The solution algorithm has been developed on the basis of a laminar Bunsen flame code [9][15]. The governing equations and boundary conditions are discretized on a two-dimensional tensor-product grid using a finite difference technique [16]. The resulting system of highly nonlinear coupled equations is solved with a damped Newton's method [17]. A preconditioned Bi-CGSTAB algorithm is used to solve the large sparse linear systems arising during Newton iterations [18].

Additionally, the numerical evaluation of the chemical production rates, thermodynamical properties, and transport coefficients imposes particular attention in order to limit the computational cost of the solution. Thus, all properties are calculated using vectorized and highly optimized gas phase chemistry, surface chemistry and transport libraries, respectively named: CHEMKIN II [19][20], SURF CHEM[5][21], and EGLIB [22].

## 2. Numerical conditions

This study aims to better understand the impact of steam, pressure and temperature on the hydrogen ignition inside PARs during a severe accident. As a first step in the investigation of this issue, in spite of the intrinsic coupling between these thermal-hydraulic quantities, we analyze independently their influence on the PAR hydrogen ignition. Then, three series of calculations with the SPARK code are conducted to study respectively the impact of steam, pressure, and temperature. Each series varies one of these parameters and keeps the two others constant. By this way, we evaluate the impact of thermal-hydraulic conditions on PAR hydrogen ignition for:

- steam concentration between 0 % and 50 %,
- pressure between 0.1 atm and 5.0 atm,
- temperature between 298 K and 423 K.

The specific inlet conditions for the investigation of the impact of steam, pressure and temperature on hydrogen ignition are detailed in the next sections.

All calculations are performed using a symmetrical and planar numerical domain which is 0.5 cm wide and 17 cm high. The catalytic plate is located at 1 cm from the inlet and it is 15 cm long. The reference grid is a regular Cartesian mesh with 26 x 86 nodes. This quite coarse grid has led to reasonable results during a grid convergence analysis. Actually, the high number of calculations necessary for this study imposes to optimize their cost in CPU time while preserving the numerical accuracy. Now, before investigating the impact of thermal-hydraulic conditions on PAR hydrogen ignition, we need to define a criterion for characterizing hydrogen ignition inside the recombiners.

## 3. Characterization of the PAR hydrogen ignition

In order to identify the PAR hydrogen ignition, we introduce two characteristic quantities respectively related to the heterogeneous (i.e. on the catalytic surface) and homogeneous (i.e. in the gas phase) hydrogen combustion:

- the total surface heat release rate:

$$Q_s^{tot} = -\int_{y_p}^{y_p+l_p} \sum_{k=1}^{n} h_k M_k \hat{\omega}_k \ , \tag{18}$$

- and the total gas phase heat release rate:

$$Q_g^{tot} = -\int_0^l \int_0^h \sum_{k=1}^{n} h_k M_k \omega_k \ , \tag{19}$$

where l is the channel length, h the channel width, $y_p$ the vertical location of the catalytic plate, and lp its length.

The PAR ignition limit is defined as the point where the heat production on the catalytic plates starts decreasing and heat production in the gaseous phase starts increasing significantly (Figure 3). Then, the hydrogen (or any relevant species) concentration at ignition is determined by the intersection of the tangent to the total gaseous heat release rate at the inflection point with the horizontal axis [14].

Figure 3 illustrates this criterion for $H_2$/Air mixtures without steam. In this example, ignition occurs at 5.4 % of hydrogen what is in good agreement with experimental data [1].

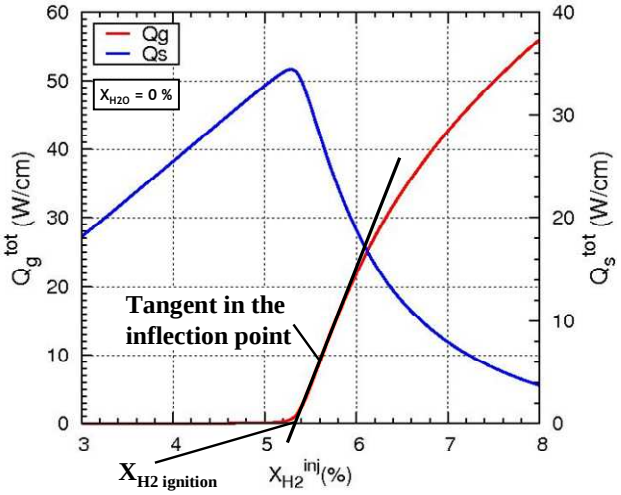


Figure 3 PAR hydrogen ignition criterion

By using the above criterion, the more detailed the solution branch is, the more accurate the ignition limit. For this reason, the code SPARK has been recently enriched by a pseudo-continuation algorithm enabling the solution branches to be automatically refined according to their curvature.

## 4. Impact of steam on the hydrogen ignition limit

The concentration of steam in the reactor containment is a key feature for the assessment of a severe accident. Its impact on the hydrogen ignition limit is one of the consequences of a low or high steam concentration.

This series of calculations aims at applying the criterion presented previously to the solution branches obtained with the numerical conditions detailed in Table 3. The inlet velocity is a typical average velocity observed at PAR inlet during the experiments. The temperature is held constant at 298 K although water can be liquid at this combination of temperature and pressure. This set of parameters is only used for a first analysis of the impact of the temperature.

Table 3 Numerical conditions for the impact of steam

| | |
|---|---|
| $T_{inj} = 298\,K$ | $\bar{p} = 1\,atm$ |
| $v_{inj} = 80\,cm/s$ | $3\% \le X_{H_2} \le 10\%$ |
| | $0\% \le X_{H_2O} \le 50\%$ |

A first qualitative analysis of the flow structure between two catalytic plates reveals the strong impact of steam on hydrogen ignition (Figure 4). Actually, while the temperature fields do not seem to be affected by the steam concentration, it appears that OH radical tends to disappear when steam concentration increases. As OH radical characterizes the homogeneous hydrogen combustion, it yields that steam can modify the ignition mechanism.

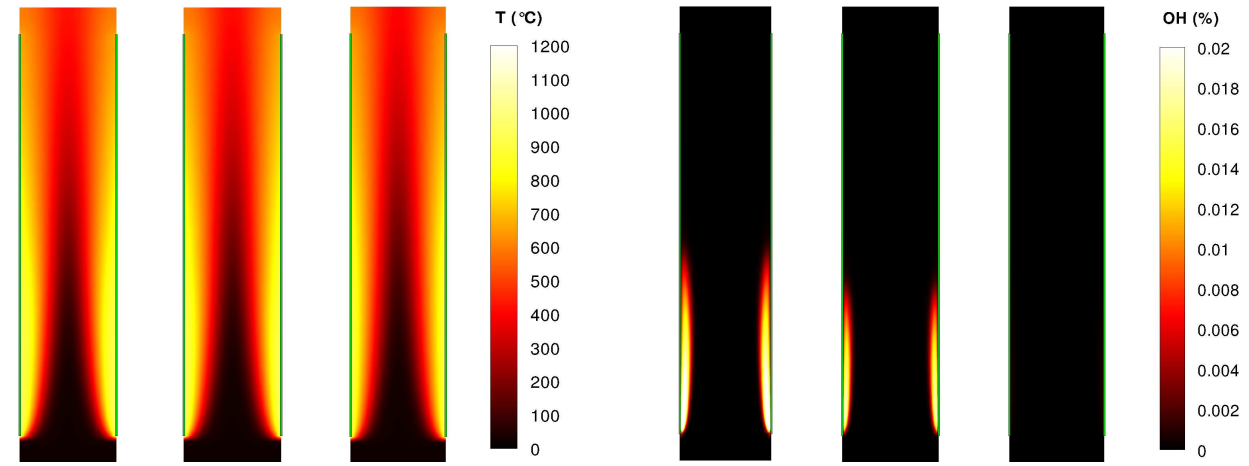


Figure 4 Impact of steam on the flow structure at 6% of hydrogen and without steam

A deeper analysis in Figure 5 confirms the significant influence of steam on the catalytic hydrogen ignition. Steam clearly delays the ignition, and therefore leads to higher hydrogen concentrations at ignition. For concentrations beyond 54 %, no ignition could be observed numerically. This result is coherent with the experimental flammability limit of hydrogen in air-steam mixtures: no ignition above 58 % of steam.

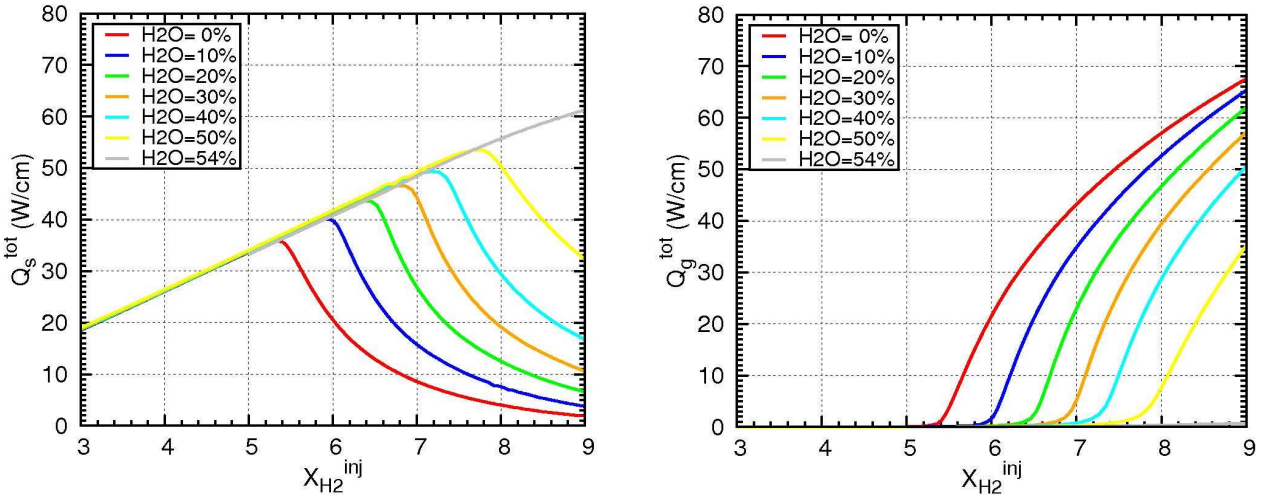


Figure 5 Impact of steam on the surface (left) and gaseous (right) total heat release rates

Table 4 gives an overview of absolute and relative shifts of the hydrogen ignition limit according to the steam concentration. Thus, by increasing the steam concentration from 0 % to 50 %, the hydrogen concentration at ignition rises by about 44 % from 5.41 % to 7.76 %.

Table 4 Impact of steam on the hydrogen ignition limit

| $X_{H2O}$ (%) | $X_{H2\ igni}$ (%) | $\Delta X_{H2}$ relative (%) |
|---|---|---|
| 0 | 5.41 | - |
| 10 | 6.00 | 10.89 |
| 20 | 6.48 | 19.87 |
| 50 | 7.76 | 43.62 |

Figure 6 presents a comparison in the ternary diagram ($H_2$, Air, $H_2O$) of the entire numerical hydrogen ignition limit with the available experimental database. It shows a good agreement between SPARK calculations and experiments. It should be noted that each numerical point in the ternary diagram results from the calculation of an entire solution branch. Therefore, the previous solution branches in Figure 5 allow defining the upper part of the PAR hydrogen limit in the ternary diagram. For more details about the procedure to establish this limit, readers are referred to [6].

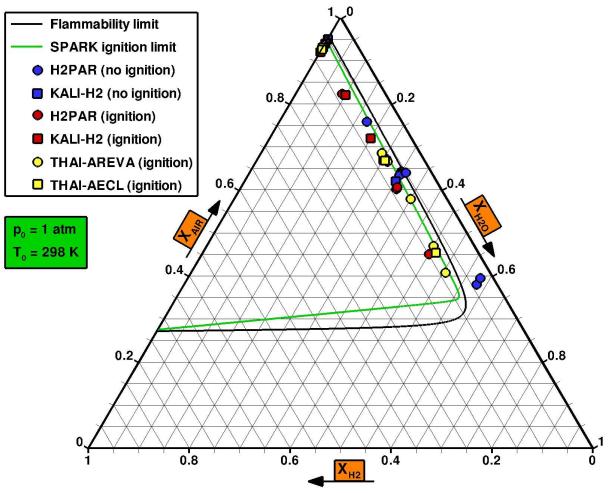


Figure 6 Hydrogen ignition limit inside PARs

## 5. Impact of pressure on the hydrogen ignition limit

The pressure inside the reactor containment is also of main importance in the assessment of a severe accident. Beyond the obvious issue related to the integrity of the containment, the pressure can affect the behavior of the recombiners, then have an impact on the standard PAR hydrogen ignition limit, and finally increase the maximum containment pressure in case of hydrogen combustion.

Table 5 Numerical conditions for the impact of pressure

| | |
|---|---|
| $T_{inj} = 298\ K$ | $0.1\ atm \le \overline{p} \le 5\ atm$ |
| $v_{inj} = 80\ cm/s$ | $3\% \le X_{H_2} \le 8\%$ |
| | $X_{H_2O} = 0\%$ |

Calculations are performed for a wide range of pressure which includes representative thermal-hydraulic conditions for PWRs and for the future ITER facility. Actually, the low containment pressure with 0.1 atm is dedicated to the ITER facility. The numerical conditions for the impact of pressure on hydrogen ignition limit inside the recombiners are listed in Table 5. The set of

parameters listed in this table does not represent realistic containment conditions, but is only used for a first analysis of the impact of the pressure.

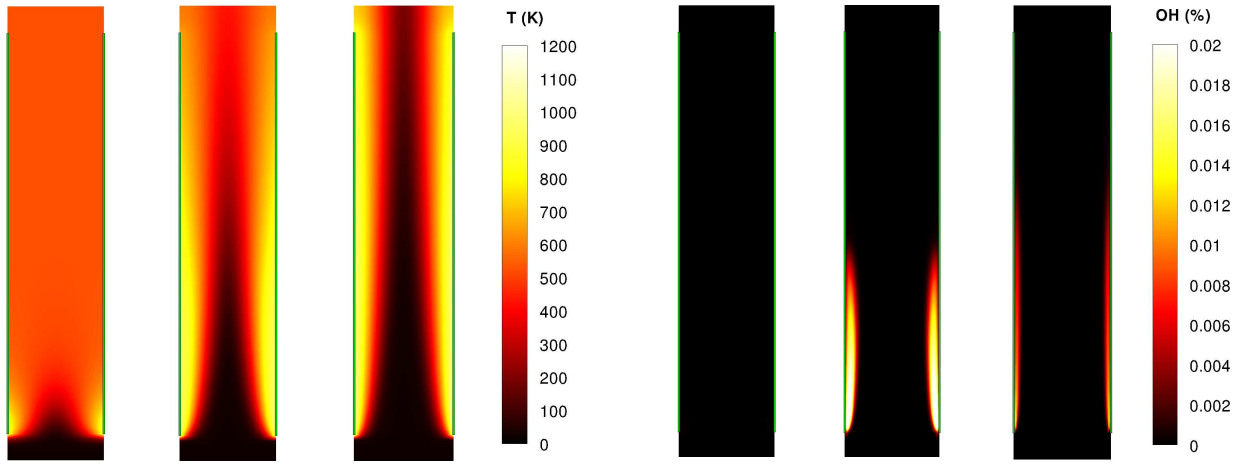


Figure 7 Impact of pressure on the flow structure at 6% of hydrogen without steam

Figure 7 illustrates the impact of pressure on the flow structure between the catalytic plates. Contrary to steam, pressure significantly modifies both the temperature and OH radical fields. In other words, the surface and gaseous heat release rates depend directly on the pressure. In fact, it appears that hydrogen ignition tends to disappear when the pressure drastically increases or decreases around the ambient pressure.

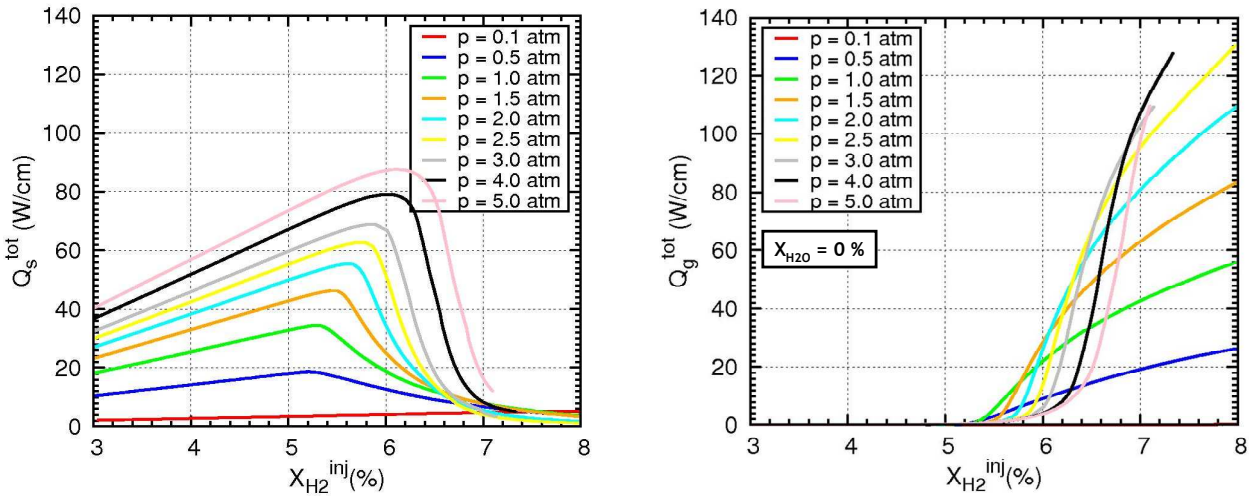


Figure 8 Impact of pressure on the surface (left) and gaseous (right) total heat release rates

Figure 8 reveals in more detail the influence of pressure on the hydrogen ignition limit inside the recombiners. At 0.1 atm no ignition could be observed numerically. At such a low pressure, only a weak catalytic activity remains on the surface (i.e. the catalytic recombination rate is roughly linear with pressure), the catalyst temperature is very low, and no homogeneous combustion can be ignited. As the pressure increases, the ignition limit is shifted to higher hydrogen concentrations.

The ignition is significantly delayed because of the higher catalytic recombination rate of hydrogen. Thus, only a low concentration of hydrogen in the gaseous phase remains, and ignition becomes progressively impossible.

Table 6 Impact of pressure on PAR hydrogen ignition limit

| p (atm) | $X_{H2\ igni}$ (%) | $\Delta X_{H2}$ relative (%) |
|---|---|---|
| 0.1 | - | - |
| 0.5 | 5.27 | -1.50 |
| 1.0 | 5.35 | 0.00 |
| 2.0 | 5.73 | 7.10 |
| 5.0 | 6.39 | 19.44 |

An overview of the absolute and relative deviations from the standard limit at 1 atm is presented in Table 6. Almost 20 % more hydrogen is necessary to ignite the mixture if the pressure is increased from 1.0 atm to 5.0 atm.

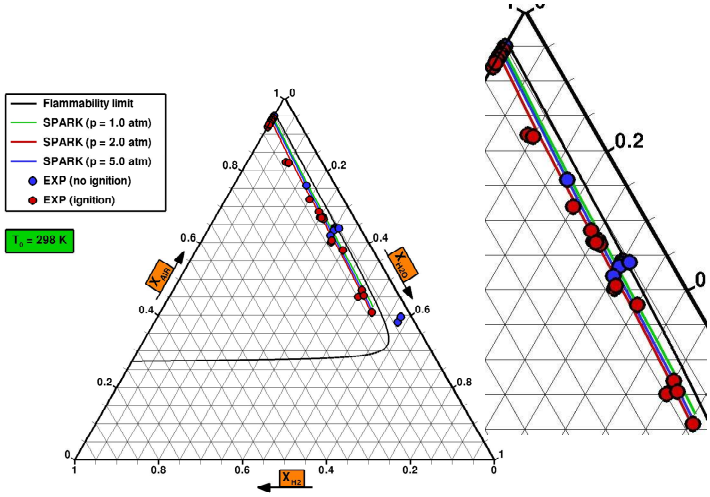


Figure 9 Impact of pressure on the hydrogen ignition limit

Figure 9 demonstrates the shift of the PAR hydrogen ignition limit to higher concentrations when pressure increases. Despite experimental data for ignition inside the recombiners are only available at 1.0 atm, the numerical results seem to be consistent. Actually, a recent experimental study on a dedicated catalytic reactor at Paul Scherrer Institute has shown the progressive extinction of catalytically stabilized hydrogen flames when pressure increases above 4 atm [23].

## 6. Impact of temperature on the hydrogen ignition limit

Temperature is the last feature considered in this study of the impact of thermal-hydraulic conditions on the hydrogen ignition inside the recombiners. The temperature inside the reactor containment, as well as the pressure, is determining for the assessment of a severe accident. Actually, the temperature can modify the behavior of recombiners, then have an impact on the standard PAR hydrogen ignition limit, and consequently increase the maximum containment pressure in case of hydrogen combustion.

Table 7 Numerical conditions for the impact of temperature

| | |
|---|---|
| $\bar{p} = 1.0\ \text{atm}$ | $298\ \text{K} \le T_{inj} \le 423\ \text{K}$ |
| $v_{inj} = 80\ \text{cm/s}$ | $3\% \le X_{H_2} \le 8\%$ |
| | $X_{H_2O} = 0\%$ |

Calculations are performed for a representative range of temperature inside PWRs. Pressure is kept constant to point out the separated effects of temperature. The numerical conditions for the impact of temperature on hydrogen ignition limit inside the recombiners are listed in Table 7.

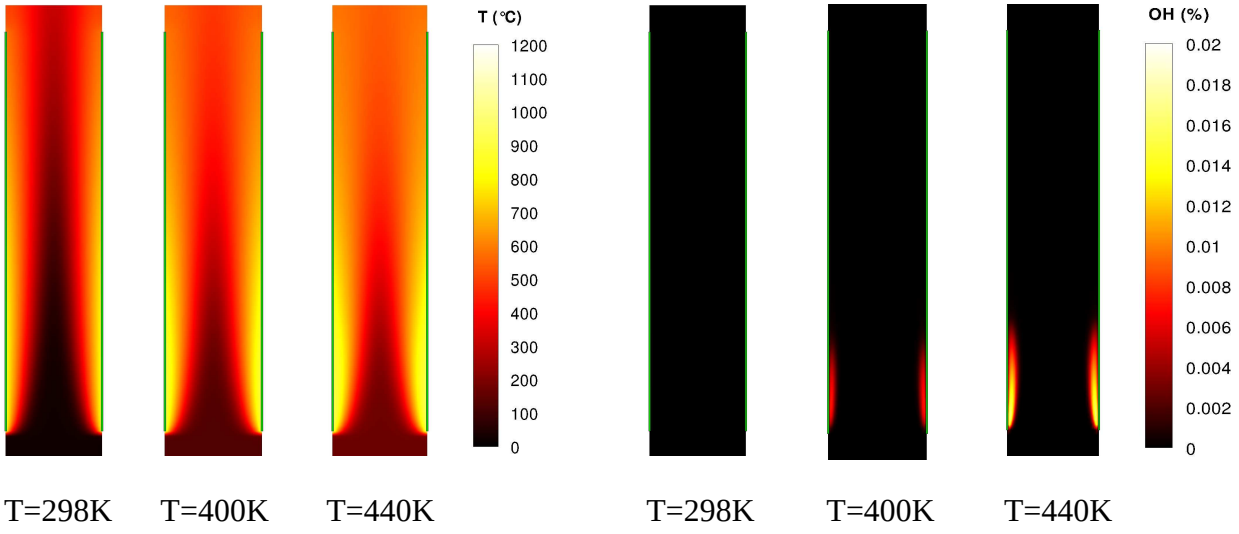


Figure 10 Impact of temperature on the flow structure at 4.8% of hydrogen without steam

As observed for the pressure, Figure 10 reveals that the temperature modifies both the temperature and OH radical fields. In fact, while there is no OH radical at ambient temperature, an increase of the inlet temperature leads to a significant production of OH radical.

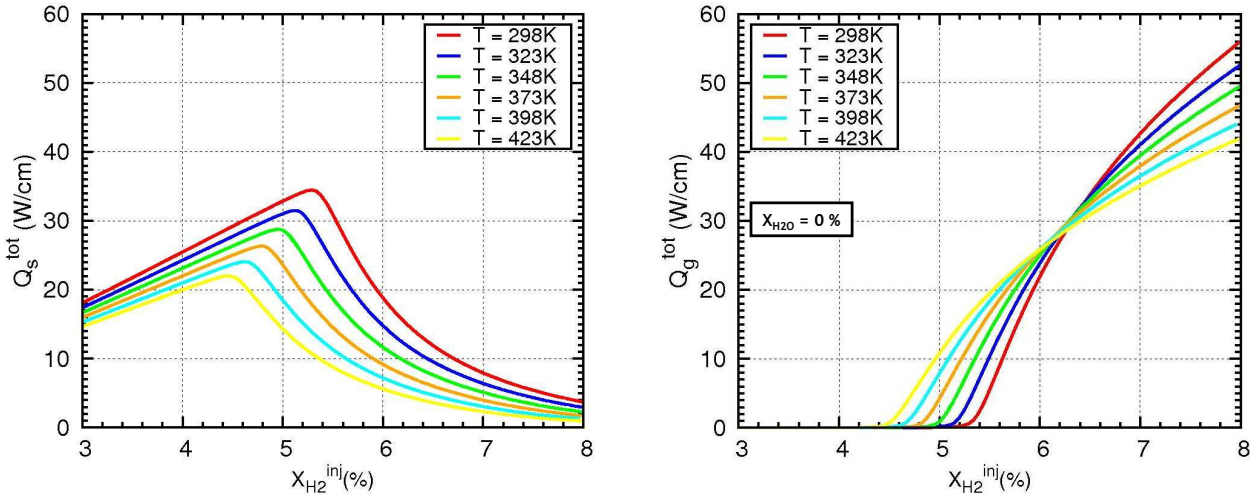


Figure 11 Impact of temperature on the surface (left) and gaseous (right) total heat release rates

Therefore, an increase of the inlet temperature seems to accelerate hydrogen ignition inside the recombiners. Actually, the inlet conditions become closer to the auto-ignition conditions in the gas phase. A deeper analysis of the impact of temperature on hydrogen ignition inside recombiners (Figure 11) shows that the inlet temperature shifts the PAR hydrogen ignition limit to lower hydrogen concentrations. Indeed, Figure 11 reveals that the surface heat release rate decreases when the temperature increases. Thus, more flammable hydrogen remains in the gas phase for similar surface temperatures, and PAR hydrogen ignition is accelerated.

Table 8 Impact of temperature on PAR hydrogen ignition limit

| T (K) | $X_{H2O\ infl}$ (%) | $\Delta X_{H2}$ relative (%) |
|---|---|---|
| 298 | 5.35 | 0 |
| 348 | 4.97 | -7.10 |
| 398 | 4.68 | -12.52 |
| 423 | 4.51 | -15.70 |

An overview of the absolute and relative deviations from the standard limit at 298 K is presented in Table 8. Almost 16 % less hydrogen is necessary to ignite the mixture if the inlet temperature is increased from 298 K to 423 K.

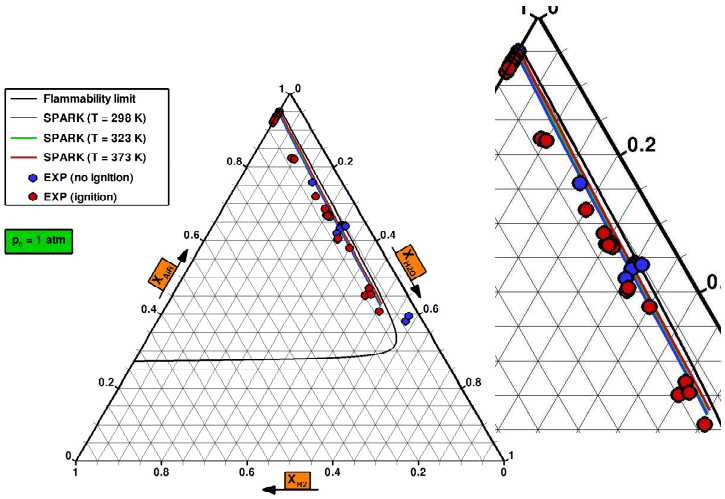


Figure 12 Impact of temperature on the hydrogen ignition limit

Finally, Figure 12 demonstrates the slight shift of the PAR hydrogen ignition limit to lower concentrations when the inlet temperature increases. Contrary to the impact of pressure on hydrogen catalytic ignition, the impact of temperature appeals experimental data to corroborate this trend.

## 7. Conclusion

This study aimed at a first analysis and understanding of the impact of the three main thermal-hydraulic parameters - steam, pressure and temperature - and their impact on the PAR ignition limit. The calculations have been performed with a dedicated numerical 2D CFD code named SPARK which is developed at IRSN.

The analyses of the impact of steam, pressure and temperature have been driven independently. Higher steam concentrations in the mixture clearly increased the hydrogen ignition concentration. Elevated pressure led to a delayed ignition of hydrogen inside PARs. This is due to the better recombination of hydrogen and oxygen on the catalytic plates which causes a lower remaining hydrogen concentration in the gaseous phase. Contrary to pressure, increased temperature accelerated the heat production in the gaseous phase and therefore the hydrogen ignition inside PARs. The higher temperature at the inlet brings the mixture closer to the auto-ignition point and therefore supports an ignition in the gaseous phase. At the same time the catalytic recombination is mitigated with increasing temperature. The numerically achieved results are confirmed by experimental observations.

In the future, coupled analyses will have to be done to study the complementary and competing influences of steam, pressure and temperature on the PAR hydrogen ignition. Additionally, investigations on the recombination of carbon monoxide and the competition between carbon monoxide and hydrogen in terms of passive autocatalytic recombination are scheduled for the near future. Due to a considerable amount of carbon monoxide produced in line with a severe accident with core meltdown in presence of concrete and other structure materials, these analyses are necessary to better prevent both hydrogen and carbon monoxide ignition.

## 8. References

[1] P. Rongier et al, “Studies of catalytic recombiner performances in H2PAR facility”, Proc. CSARP, Bethesda, USA, May 5-8, (1997).

[2] O. Braillard, “Test of passive catalytic recombiners (PARs) for combustible gas control in nuclear power plants”, Proc. 2nd International Topical Meeting on Advanced Reactor Safety ARS, Vol. 97, pp. 541-548, (1997).

[3] G. Poss et al, “Experimental investigation of passive autocatalytic recombiner (PAR) units under accidental scenarios”, Proc. 2nd International Topical Meeting on Safety and Technology of Nuclear Hydrogen Production, Control, and Management, American Nuclear Society, San Diego, California, June, (2010).

[4] A. Bentaïb et al, “Evaluation of the impact that PARs have on the hydrogen risk in the reactor containment: methodology and application to PSA level 2”, Proc. TOPSAFE, Dubrovnik, Croatia, Sept. 30 - Oct. 3, (2008).

[5] N. Meynet, A. Bentaib, “SPARK - Logiciel de calcul pour les recombineurs catalytiques Version 1.0”, IRSN, Technical Report DSR/SAGR/03, (2008).

[6] N. Meynet, A. Bentaib, “Numerical Study of Hydrogen Ignition by Passive Auto-catalytic Recombiners”, Proc. Second International Meeting of the Safety and Technology of Nuclear Hydrogen Production, Control and Management, American Nuclear Society, San Diego, USA, June 13-16, (2010).

[7] S.B. Dworkin, B.A.V. Bennett, and M.D. Smooke, “A mass-conserving vorticity-velocity formulation with application to non-reacting and reacting flows”, *Journal of Computational Physics*, Vol. 215, pp. 430-447, (2006).

[8] A. Ern and M.D. Smooke, "Vorticity-Velocity Formulation for Three-Dimensional Steady Compressible Flows", *Journal of Computational Physics*, Vol. 105, pp. 58-71, (1993).

[9] V. Giovangigli, "Multicomponent Flow Modeling", Birkhauser Ed., Boston, (1999).

[10] A. Ern, V. Giovangigli, "Fast and Accurate Multicomponent Transport Property Evaluation", *Journal of Computational Physics*, Vol. 120, pp. 105-116, (1995).

[11] J. Warnatz, R.W. Dibble, U. Mass, "Combustion, Physical and Chemical Fundamentals, Modeling and Simulation", Springer-Verlag Ed., New York, (1996).

[12] O. Deutschmann et al, "Numerical modeling of catalytic ignition", Twenty-Sixth Symposium (International) on Combustion, Edition The Combustion Institute, pp. 1747-1754, (1996).

[13] G. Bergeret, "Characterization of metallic catalysts by X-ray and electron microscopy techniques", in Catalysis by metals, Les Editions de Physique Ed., pp 167-180, (1997).

[14] C. Appel et al, "An Experimental and Numerical Investigation of Homogeneous Ignition in Catalytically Stabilized Combustion of Hydrogen-Air Mixtures over Platinum", *Combustion and Flame*, 128, pp. 340-368, (2002).

[15] N. Meynet, "Simulation numérique de la combustion d'un propergol solide", Ph.D. Thesis, Paris 6 University, (2005).

[16] A. Ern, C.C. Douglas, M.D. Smooke, "Detailed chemistry modeling of laminar diffusion flames on parallel computers", The International Journal of Supercomputer Applications, Vol. 9, n°3, pp. 167-186, (1995).

[17] P. Deuflhard, "A Modified Newton Method for the Solution of Ill-Conditioned Systems of Nonlinear Equations with Application To Multiple Shooting", Numerical Mathematics, Springer Verlag Ed., Vol. 22, pp. 289-315, (1974).

[18] A. Ern et al, "Towards Polyalgorithmic Linear System Solvers For Nonlinear Elliptic Problems", *SIAM Journal on Scientific Computing*, Vol. 15, n°3, pp. 681–703, (1994).

[19] V. Giovangigli, N. Darabiha, "Vector computers and complex chemistry combustion", Mathematical Modeling in Combustion and Related Topics, C. Brauner and C. Schmidt-Laine Ed., Vol. 140, pp. 491-503, (1988).

[20] R.J. Kee, F.M. Rupley, and J.A. Miller, "CHEMKIN II: A Fortran Chemical Kinetics Package for the Analysis of Gas Phase Chemical Kinetics", Sandia National Laboratories, Technical Report SAND89-8009B, (1989).

[21] R.J. Kee et al, "SURFACE CHEMKIN: A Software Package for the Analysis of Heterogeneous Chemical Kinetics at a Solid-Surface - Gas-Phase Interface", CHEMKIN Collection Release 3.6, Reactor Design Inc., San Diego, (2000).

[22] A. Ern and V. Giovangigli, "EGLIB: A general purpose Fortran library for multicomponent transport property evaluation", CERMICS, Technical report n° 96-51, (1996).

[23] J. Mantzaras, R. Bombach and R. Schaeren, "Hetero-/homogeneous combustion of hydrogen/air mixtures over platinum at pressures up to 10 bar", Proceedings of the Combustion Institute, Vol. 32, n°2, pp. 1937-1945, (2009).